J. Fluid Mech. (1994), *vol.* 262, *pp.* 1–26

The motion generated by a slowly rising disk in an unbounded rotating fluid for arbitrary Taylor number

By D. VEDENSKY AND M. UNGARISH†
Department of Computer Science, Technion, Haifa 32000, Israel

(Received 19 April 1993 and in revised form 18 August 1993)

The motion of a disk rising steadily parallel to the axis of rotation in a uniformly rotating unbounded liquid is considered. In the limit of zero Rossby number the linear viscous equations of motion are reduced to a system of dual integral equations which renders an 'exact' solution for arbitrary values of the Taylor number, *Ta*. The investigation is focused on the drag and the flow field. In the limits of small and large *Ta* the asymptotic results of the present formulation agree with – and extend – previous investigations by different approaches.

A particular novel feature, for large *Ta*, is the contribution of the Ekman-layer flux to the outer motion. New insight into the structure of the Taylor column is gained; in particular, it is shown that the main part of the column is a 'bubble' of recirculating fluid, detached from the body and not communicating with the Ekman layer. However, it turns out that the essential discrepancy in drag between experiments (Maxworthy 1970) and previous theories cannot be attributed to the Ekman-layer suction effect.

1. Introduction

The motion of a particle in a rotating fluid, parallel to the axis of rotation, is of interest from several points of view. This is a fundamental problem in the theory of 'unbounded' rotating fluids, which has important counterparts in the theory of stratified and conducting fluids, and essential implications for the modelling of rotating two-phase suspensions (Ungarish 1993). A theoretical background is given in Greenspan (1968, in particular Chap. 4). Without going into the historical details of the many pertinent investigations, we shall point out here some important outcomes relevant to the present work.

The equations governing the motion of an incompressible viscous fluid, in a system rotating with constant angular velocity Ω^*, are the conservation of mass and momentum:

$$\nabla \cdot \boldsymbol{v}^* = 0, \tag{1}$$

$$\frac{\partial \boldsymbol{v}^*}{\partial t^*} + \boldsymbol{v}^* \cdot \nabla \boldsymbol{v}^* + 2\boldsymbol{\Omega}^* \times \boldsymbol{v}^* = -\frac{\nabla P^*}{\rho^*} - \nu^* \nabla \times \nabla \times \boldsymbol{v}^*. \tag{2}$$

Here $\boldsymbol{v}^*$ is the velocity in the rotating coordinate system, P^* is the reduced pressure, t^* time, ρ^* and ν^* are the density and kinematic viscosity of the fluid; a^* and V^* denote the radius and velocity of the particle. Asterisks denote dimensional variables.

† To whom correspondence should be addressed.

To non-dimensionalize (1) and (2) the following scaling is utilized:

$$\{\boldsymbol{r}^*, t^*, \boldsymbol{v}^*, P^*\} = \left\{a^*\boldsymbol{r}, \Omega^{*-1}t, V^*\boldsymbol{v}, \frac{V^*\nu^*\rho^*}{a^*}P\right\}. \tag{3}$$

Now the governing equations read

$$\nabla\cdot\boldsymbol{v} = 0, \tag{4}$$

$$\frac{\partial\boldsymbol{v}}{\partial t} + (Ro\,Ta)\,\boldsymbol{v}\cdot\nabla\boldsymbol{v} + 2Ta(\hat{z}\times\boldsymbol{v}) = -\nabla P - \nabla\times\nabla\times\boldsymbol{v}, \tag{5}$$

where $\hat{z}$ is the unit vector in the direction of the axis of rotation.

Two independent dimensionless parameters highlight the flow field generated by the motion of the particle:

$$Ta = \frac{a^{*2}\Omega^*}{\nu^*}, \quad Ro = \frac{V^*}{\Omega^* a^*}, \tag{6a}$$

and their combination is

$$Re = Ro\,Ta = a^*V^*/\nu^*. \tag{6b}$$

The Taylor number, Ta, expresses the typical ratio of the Coriolis to the viscous force in the fluid (Ta is actually the inverse of the Ekman number of the particle). The Rossby number, Ro, a ratio of the convective to the Coriolis accelerations, estimates the relative importance of nonlinear terms. The Reynolds number, Re, has the usual interpretation.

Setting $Ro = 0$ in (5) yields the important linear formulation, which we adopt here. The boundary conditions are no-penetration and no-slip on the particle, whose geometry is specified, and free-stream velocity at infinity.

Two limiting linear cases have been studied in detail: the slightly viscous rapid rotation, $Ta\to\infty$, and the viscous slow rotation, $Ta\to 0$.

The solution of the linear, steady-state rapidly rotating and inviscid ($Ta^{-1} = 0$) problem is not unique.

Stewartson (1952) obtained a formal complete solution of the linear, time-dependent, inviscid ($Ta^{-1} = 0$) case of an ellipsoid starting impulsively from rest. Here the momentum balance is between the time-dependent, Coriolis and pressure terms. In the steady-state limit the drag on a circular particle such as a sphere or a disk is given by

$$D^* = \tfrac{16}{3}\Omega^* a^{*3} V^* \rho^*. \tag{7}$$

The corresponding flow field is an infinitely long column of swirling fluid moving with the particle, identified as the Taylor column. The swirl velocity is infinite and discontinuous on the cylindrical boundary of this column. The detailed time-dependent solution of the analogous problem for a disk was presented by Greenspan (1968, Sect. 4.3).

Morrison & Morgan (1956) considered the steady, rapidly rotating, slightly viscous ($Ta \gg 1$) flow field around a disk. Their report was distributed but apparently unpublished, and the main results are mostly known from the re-derivation, with due credit, in Moore & Saffman (1969, section 8). Therefore the latter is commonly used as a reference and we shall follow this trend. In this solution the main approximation was that the z-derivatives in the shear terms were discarded, so that no 'horizontal' Ekman layer could appear and the no-slip conditions could not be imposed. (It can be argued that the results are essentially correct also for a sphere.) However, the non-

physical discontinuity of Stewartson's solution at the lateral surfaces of the Taylor column is removed by the retained viscous effects. The drag is the same as the above-mentioned Stewartson's result, (7). An important feature in this solution is the finite axial extent of the Taylor column; as pointed out by Barnard & Pritchard (1975), the stagnation point of the axial velocity (with respect to the body) yields this length as $0.052Ta$ (in dimensionless form). This will be discussed in more detail in §4.

The opposite limit of Ta has been investigated by perturbations around the Stokesian (creeping) non-rotating flow, $Ta = 0$, which yielded the well-known formula

$$D^* = 6\pi\nu^*\rho^*a^*V^* \tag{8}$$

for a sphere. The corresponding result for a disk translating along its axis (see Ray 1936) is

$$D^* = 16\nu^*\rho^*a^*V^*. \tag{9}$$

The analysis of Childress (1964) for a spherical particle moving parallel to the axis of rotation, assuming $Ta \ll 1$, resulted in

$$D^* = 6\pi\nu^*\rho^*a^*V^*(1+\tfrac{4}{7}Ta^{\frac{1}{2}}). \tag{10}$$

A similar dependency on Ta was predicted for other circular geometries, as discussed later. The numerical solutions of the full Navier–Stokes equations presented by Dennis, Ingham & Singh (1982) provide support and additional information on the drag and the flow field for the range $Ta \leqslant 0.5$, $0.05 \leqslant Re \leqslant 0.5$ (note that $Ro \geqslant 0.1$).

The intermediate range $Ta = O(1)-O(100)$ defies simplification and has therefore received little theoretical attention. Weisenborn (1985) used the special method of induced forces to calculate the drag on a sphere for arbitrary Ta, but gave no information on the flow field. Dennis *et al.* (1982) could not obtain reliable numerical solutions in this range because of difficulties of satisfying the boundary conditions as the computational domain elongates.

Experiments on a spherical particle in different ranges of parameters were performed by Taylor (1922) and Maxworthy (1965, 1970). The latter combined the determination of the drag with observation of the flow field. We note that similar experimental results for the disk configuration are not available, to the best of our knowledge, perhaps because of additional practical difficulties that may occur in producing a stable broadside motion of a very thin body.

The theoretical drag for small Ta (actually, up to 0.75) is in good agreement with the measurements. Comparisons in the intermediate range have not been performed.

The situation for large Ta appears to be rather perplexing. Maxworthy (1970) reported drag values much larger (about 50%) than the theoretical predictions. On the other hand, the length of the 'slug' (Taylor column) turned out to be consistent with the results of Moore & Saffman (1969) (this was actually pointed out by Barnard & Pritchard 1975).

Three factors were suspected as causes of this discrepancy: (i) the wall effect (from the 'horizontal' top and bottom of the container) on the flow field, not accounted for in the theoretical consideration; (ii) the omission of the Ekman layers and of the associate no-slip boundary conditions in the theoretical consideration of Moore & Saffman; (iii) the omission of the convective terms (linearization of the equations), since the 'small' Ro in the experiments was of order 0.01–0.1, perhaps not small enough.

Hocking, Moore & Walton (1979) incorporated the influence of 'horizontal' boundaries in Moore & Saffman's (1969) analysis (again, the no-penetration is accounted for, but no Ekman layers are incorporated). The conclusion was that this

wall effect yields a relatively small increase of drag in the configuration tested by Maxworthy (1970), substantially below the reported discrepancy.

The influence of the Ekman layer remained largely unclear. Maxworthy (1970) suggested that the fluid within the stagnant 'slug' was drawn into the Ekman layer; but he also mentions that 'No attempt has been made to calculate the more complicated interaction problem defined when the effect of the Ekman boundary-layer flux on the outer flow is to be found. It is well known that such effects are of great importance in rotating flows, but they are not sufficiently well understood to allow a quantitative, or even qualitative, extension to the present case'. In this context, it is also worth mentioning that the 'slug', extensively referred to by many investigators, remained basically obscure regarding the flow inside (i.e. whether the fluid in this domain is slowly flowing or recirculating, or both). Consequently, from the analytical point of view the boundaries of the 'slug' have not been defined, and only the tip of it has been identified in a rather *ad hoc* manner as the position of the farthest stagnation point on the axis.

The present investigation attempts to throw some new light on the problem via the exact solution of the full linear system for the steady-state flow field past a rising disk for arbitrary values of Ta; the Ekman layers are implicitly accounted for when $Ta \gg 1$, and the drag, at any Ta, is a straightforward product.

Although the disk is formally less interesting than the sphere, the present work advances knowledge in several aspects: an exact solution for the flow field and drag is provided; the previous approximate solutions for small Ta are confirmed and extended; the flow field for the moderate-Ta range is covered; for large Ta the contribution of the Ekman layers to the structure of the Taylor column is established. However, no substantial modification of the drag for large Ta was found, so that the unexplained discrepancy with Maxworthy's measurements appears to be either an experimental error or a paradox.

The outline of this paper is as follows. In §2 the governing equations are reduced to a system of dual integral equations and the formal solution of the problem is obtained. Evaluation of the drag with respect to Ta is performed in §3. Section 4 describes the flow field, and a discussion of present results versus previous knowledge is presented in §5.

2. Formal solution

In view of the axial symmetry, the scalar form of the governing equations (4) and (5) is

$$-2Tav = -\frac{\partial P}{\partial r} + \left(\frac{\partial^2 u}{\partial r^2} + \frac{\partial u}{r\,\partial r} - \frac{u}{r^2} + \frac{\partial^2 u}{\partial z^2}\right), \tag{11}$$

$$2Tau = \left(\frac{\partial^2 v}{\partial r^2} + \frac{\partial v}{r\,\partial r} - \frac{v}{r^2} + \frac{\partial^2 v}{\partial z^2}\right), \tag{12}$$

$$0 = -\frac{\partial P}{\partial z} + \left(\frac{\partial^2 w}{\partial r^2} + \frac{\partial w}{r\,\partial r} + \frac{\partial^2 w}{\partial z^2}\right), \tag{13}$$

$$\frac{\partial (ru)}{r\,\partial r} + \frac{\partial w}{\partial z} = 0. \tag{14}$$

Here r and z are the radius and axial coordinate in a cylindrical frame attached to the centre of the disk and rotating with the unperturbed fluid, and $\boldsymbol{v} = \{u, v, w\}$. To close

the boundary value problem the conditions on the disk and at infinity should be specified. Since the equations do not contain convection terms and the domain is unbounded, no rotation of the torque-free disk relative to the embedding fluid is possible. Hence

$$u = v = w = 0 \quad \text{at} \quad 0 \leqslant r \leqslant 1, \quad z = 0; \tag{15}$$

$$u = v = 0; \quad w = -1 \quad \text{at} \quad r^2 + z^2 \to \infty. \tag{16}$$

The solution of the system is attempted using the Hankel transform:

$$\bar{\mathrm{f}}(p) = \int_0^\infty \mathrm{f}(r)\, r J_1(pr)\, \mathrm{d}r, \tag{17}$$

$$\mathrm{f}(r) = \int_0^\infty \bar{\mathrm{f}}(p)\, p J_1(rp)\, \mathrm{d}p, \tag{18}$$

where p is the parameter of the transform (not to be confused with the pressure P).

Differentiation of (13) and (14) with respect to r and application of (17) yields

$$-2Ta\,\bar{v} = -\overline{\left(\frac{\partial P}{\partial r}\right)} + \left(-p^2 + \frac{\partial^2}{\partial z^2}\right)\bar{u}, \tag{19}$$

$$2Ta\,\bar{u} = \left(-p^2 + \frac{\partial^2}{\partial z^2}\right)\bar{v}, \tag{20}$$

$$-\frac{\partial}{\partial z}\overline{\left(\frac{\partial P}{\partial r}\right)} + \left(-p^2 + \frac{\partial^2}{\partial z^2}\right)\overline{\left(\frac{\partial w}{\partial r}\right)} = 0, \tag{21}$$

$$-p^2\bar{u} + \frac{\partial}{\partial z}\overline{\left(\frac{\partial w}{\partial r}\right)} = 0. \tag{22}$$

Differentiation of (21) with respect to z and elimination of $\overline{(\partial P/\partial r)}$ and $(\partial/\partial z)\overline{(\partial w/\partial r)}$ by virtue of (19) and (22) produces

$$2Ta\frac{\partial^2 \bar{v}}{\partial z^2} = -\left(\frac{\partial^2}{\partial z^2} - p^2\right)^2 \bar{u}. \tag{23}$$

Combining (23) with (20) yields

$$4Ta^2\frac{\partial^2 \bar{v}}{\partial z^2} + \left(\frac{\partial^2}{\partial z^2} - p^2\right)^3 \bar{v} = 0, \tag{24}$$

which is essentially a sixth-order ordinary differential equation for $\bar{v}(z)$, with p treated as a parameter. Its characteristic equation is

$$4Ta^2 Z^2 + (Z^2 - p^2)^3 = 0. \tag{25}$$

This sixth-order equation can be easily reduced to a third-order one by introducing a new variable λ and a parameter s:

$$\lambda = \frac{Z^2}{p^2} - 1, \quad s = \frac{4Ta^2}{p^4}. \tag{26}$$

Now the characteristic equation reads

$$\lambda^3 + s\lambda + s = 0; \tag{27}$$

its three roots, by Cardano's formula, are

$$\lambda_1 = \epsilon_1 + \epsilon_2, \tag{28}$$

$$\lambda_2 = -\tfrac{1}{2}(\epsilon_1 + \epsilon_2) + \tfrac{1}{2}\mathrm{i}\sqrt{3}\,(\epsilon_1 - \epsilon_2), \tag{29}$$

$$\lambda_3 = -\tfrac{1}{2}(\epsilon_1 + \epsilon_2) - \tfrac{1}{2}\mathrm{i}\sqrt{3}\,(\epsilon_1 - \epsilon_2), \tag{30}$$

where

$$\epsilon_1 = \left[-\tfrac{1}{2}s + \left(\frac{s^3}{27} + \frac{s^2}{4} \right)^{\frac{1}{2}} \right]^{\frac{1}{3}}, \tag{31}$$

$$\epsilon_2 = \left[-\tfrac{1}{2}s - \left(\frac{s^3}{27} + \frac{s^2}{4} \right)^{\frac{1}{2}} \right]^{\frac{1}{3}}. \tag{32}$$

The general solutions of (24), decaying for $z \to \infty$ and $z \to -\infty$, read

$$\bar{v}^T = \alpha^T(p, Ta)\,\mathrm{e}^{-p(1+\lambda_1)^{\frac{1}{2}}z} + \beta^T(p, Ta)\,\mathrm{e}^{-p(1+\lambda_2)^{\frac{1}{2}}z} + \gamma^T(p, Ta)\,\mathrm{e}^{-p(1+\lambda_3)^{\frac{1}{2}}z}, \tag{33}$$

$$\bar{v}^B = \alpha^B(p, Ta)\,\mathrm{e}^{p(1+\lambda_1)^{\frac{1}{2}}z} + \beta^B(p, Ta)\,\mathrm{e}^{p(1+\lambda_2)^{\frac{1}{2}}z} + \gamma^B(p, Ta)\,\mathrm{e}^{p(1+\lambda_3)^{\frac{1}{2}}z}. \tag{34}$$

Hereafter, the superscripts T and B denote solutions for $z \geqslant 0$ and $z \leqslant 0$ respectively (top, bottom). Substitution of (33) into (18) produces, for the physical variable v at the upper (upstream) half-space ($z \geqslant 0$),

$$v^T = \int_0^\infty pJ_1(rp)\left[\alpha^T \mathrm{e}^{-p(1+\lambda_1)^{\frac{1}{2}}z} + \beta^T \mathrm{e}^{-p(1+\lambda_2)^{\frac{1}{2}}z} + \gamma^T \mathrm{e}^{(1+\lambda_3)^{\frac{1}{2}}z}\right] \mathrm{d}p. \tag{35}$$

Utilization of the results for v in (12) gives the following values for the u-component:

$$u^T = \frac{1}{2Ta}\int_0^\infty p^3 J_1(rp)\left[\alpha^T\lambda_1 \mathrm{e}^{-p(1+\lambda_1)^{\frac{1}{2}}z} + \beta^T\lambda_2 \mathrm{e}^{-p(1+\lambda_2)^{\frac{1}{2}}z} + \gamma^T\lambda_3 \mathrm{e}^{-p(1+\lambda_3)^{\frac{1}{2}}z}\right] \mathrm{d}p. \tag{36}$$

Substitution of (36) into (14) and subsequent integration on account of (16) give

$$w^T = -1 + \frac{1}{2Ta}\int_0^\infty p^3 J_0(rp)\left[\alpha^T \frac{\lambda_1}{(1+\lambda_1)^{\frac{1}{2}}} \mathrm{e}^{-p(1+\lambda_1)^{\frac{1}{2}}z} + \beta^T \frac{\lambda_2}{(1+\lambda_2)^{\frac{1}{2}}} \mathrm{e}^{-p(1+\lambda_2)^{\frac{1}{2}}z} + \gamma^T \frac{\lambda_3}{(1+\lambda_3)^{\frac{1}{2}}} \mathrm{e}^{-p(1+\lambda_3)^{\frac{1}{2}}z}\right] \mathrm{d}p. \tag{37}$$

The appropriate formulae for the velocity components u and v in the half-space $z \leqslant 0$ are similar: the superscript T should be replaced by B and $-$ in the exponents by $+$; also, for w the sign before the integral should be changed to $-$.

Hence, to evaluate the flow field the six unknown functions α^T, α^B, β^T, β^B, γ^T, and γ^B are to be determined.

The form of the governing equations and the symmetry of the configuration suggest symmetry relationships about the plane of the disk in the flow field considered, i.e.

$$u(r, z) = -u(r, -z), \quad v(r, z) = -v(r, -z) \quad w(r, z) = w(r, -z). \tag{38}$$

These three requirements, on account of (35)–(37), and their counterparts for $z \leqslant 0$ are consistent and equivalent, in turn, to

$$\alpha^T = -\alpha^B, \quad \beta^T = -\beta^B, \quad \gamma^T = -\gamma^B. \tag{39}$$

Denote

$$\alpha = \alpha^T, \quad \beta = \beta^T, \quad \gamma = \gamma^T. \tag{40}$$

Hence, α, β, and γ are the three unknown functions left instead of six. Further progress is based on additional use of (38). They readily imply

$$u(r, z=0) = v(r, z=0) = 0. \tag{41}$$

Since (41) is true for any r, it imposes, via (35) and (36), the conclusion

$$\alpha+\beta+\gamma = 0, \tag{42}$$

$$\lambda_1\alpha+\lambda_2\beta+\lambda_3\gamma = 0. \tag{43}$$

Solving for β and γ in terms of α:

$$\beta = \alpha\frac{\lambda_1-\lambda_3}{\lambda_3-\lambda_2}, \quad \gamma = \alpha\frac{\lambda_2-\lambda_1}{\lambda_3-\lambda_2}, \tag{44}$$

reduces the number of unknown functions to one, $\alpha(p, Ta)$.

For further progress the pressure has to be determined. In view of (35) and (36), prescribing $P = 0$ at $r^2+z^2 \to \infty$, (11) yields for $z \geqslant 0$

$$P = -\int_0^\infty J_0(rp)\left\{\alpha\left[2Ta+\frac{p^4}{2Ta}\lambda_1^2\right]e^{-p(1+\lambda_1)^{\frac{1}{2}}z}+\beta\left[2Ta+\frac{p^4}{2Ta}\lambda_2^2\right]e^{-p(1+\lambda_2)^{\frac{1}{2}}z}\right.$$
$$\left.+\gamma\left[2Ta+\frac{p^4}{2Ta}\lambda_3^2\right]e^{-p(1+\lambda_3)^{\frac{1}{2}}z}\right\}dp. \tag{45}$$

In view of (38) it is easily seen from the equations of motion that

$$P(r, -z) = -P(r, z). \tag{46}$$

In particular, in the plane of the disk, in view of (42), the pressure is

$$P(r, z=0^+) = -\frac{1}{2Ta}\int_0^\infty p^4 J_0(rp)\,[\alpha\lambda_1^2+\beta\lambda_2^2+\gamma\lambda_3^2]\,dp. \tag{47}$$

It is useful also to evaluate the stream function, $\psi(r, z)$. Prescribing $\psi = 0$ on the axis (hence also on the disk), and on account of (37), for the upper half-space, one obtains

$$\psi = \int_0^r rw(r, z)\,dr = -\frac{r^2}{2}+\frac{1}{2Ta}\int_0^\infty rp^2 J_1(rp)$$
$$\times\left[\alpha\frac{\lambda_1}{(1+\lambda_1)^{\frac{1}{2}}}e^{-p(1+\lambda_1)^{\frac{1}{2}}z}+\beta\frac{\lambda_2}{(1+\lambda_2)^{\frac{1}{2}}}e^{-p(1+\lambda_2)^{\frac{1}{2}}z}+\gamma\frac{\lambda_3}{(1+\lambda_3)^{\frac{1}{2}}}e^{-p(1+\lambda_3)^{\frac{1}{2}}z}\right]dp. \tag{48}$$

To determine α a system of dual integral equations is formulated. The first equation expresses the no-penetration requirement on the disk surface, which, by virtue of (37) for $z = 0$, reads

$$\frac{1}{2Ta}\int_0^\infty p^3 J_0(rp)\left[\frac{\lambda_1}{(1+\lambda_1)^{\frac{1}{2}}}+\frac{\lambda_2}{(1+\lambda_2)^{\frac{1}{2}}}\frac{\lambda_1-\lambda_3}{\lambda_3-\lambda_2}+\frac{\lambda_3}{(1+\lambda_3)^{\frac{1}{2}}}\frac{\lambda_2-\lambda_1}{\lambda_3-\lambda_2}\right]\alpha(p, Ta)\,dp = 1,$$
$$\text{for} \quad 0 \leqslant r < 1. \tag{49}$$

The complementary equation is based on the pressure continuity at $z = 0$, $r > 1$, which, in view of the symmetry (46), implies

$$P(r, z=0) = 0 \quad \text{for} \quad r > 1. \tag{50}$$

On account of (47) and (44), (50) yields

$$\int_0^\infty p^4 J_0(rp)\left[\lambda_1^2+\lambda_2^2\frac{\lambda_1-\lambda_3}{\lambda_3-\lambda_2}+\lambda_3^2\frac{\lambda_2-\lambda_1}{\lambda_3-\lambda_2}\right]\alpha(p, Ta)\,\mathrm{d}p = 0 \quad \text{for} \quad r > 1. \tag{51}$$

Equations (49) and (51) form the dual integral equations for α as a function of p for any given Ta. The solution is attempted by the method suggested by Tranter (1951), as follows. In general, consider the dual integral equations

$$\int_0^\infty \tilde{G}(p) f(p) J_0(rp)\,\mathrm{d}p = A, \quad 0 < r < 1, \tag{52}$$

$$\int_0^\infty f(p) J_0(rp)\,\mathrm{d}p = 0, \quad r > 1, \tag{53}$$

where $f(p)$ is the unknown function, $\tilde{G}(p)$ is a prescribed function and A a given parameter. Tranter showed that the system (52), (53) is satisfied by

$$f(p) = p^{1-k}\sum_{m=0}^{\infty} a_m J_{2m+k}(p), \tag{54}$$

where the coefficients a_m are prescribed by the linear system:

$$a_0 + \sum_{m=0}^{\infty} L_{0,m}\, a_m = \frac{2^{1-k}}{\Gamma(k)}A, \tag{55}$$

$$a_n + \sum_{m=0}^{\infty} L_{n,m}\, a_m = 0 \quad \text{for} \quad n \geqslant 1, \tag{56}$$

where

$$L_{n,m} = (4n+2k)\int_0^\infty [p^{2-2k}\tilde{G}(p) - 1]p^{-1} J_{2m+k}(p) J_{2n+k}(p)\,\mathrm{d}p. \tag{57}$$

Formally, the parameter $k > 0$ can be chosen rather arbitrarily, subject to the restriction that the improper integrals $L_{n,m}$ converge. However, in particular applications the 'proper' and perhaps unique choice of k is essential, as seen later.

Comparing our problem, which is described by the dual integral equations (49) and (51), with the general one (52), (53), it is readily seen that by identifying

$$A = 2, \quad \tilde{G}(p) = -\frac{2\,\theta(p)}{p\,\eta(p)}, \quad f(p) = -\frac{p^4 \eta(p)\,\alpha(p)}{2Ta}, \tag{58}$$

where

$$\theta(p) = \frac{\lambda_1}{(1+\lambda_1)^{\frac{1}{2}}}+\frac{\lambda_2}{(1+\lambda_2)^{\frac{1}{2}}}\frac{\lambda_1-\lambda_3}{\lambda_3-\lambda_2}+\frac{\lambda_3}{(1+\lambda_3)^{\frac{1}{2}}}\frac{\lambda_2-\lambda_1}{\lambda_3-\lambda_2}, \tag{59}$$

$$\eta(p) = \frac{\lambda_1^2(\lambda_3-\lambda_2)+\lambda_2^2(\lambda_1-\lambda_3)+\lambda_3^2(\lambda_2-\lambda_1)}{\lambda_3-\lambda_2}, \tag{60}$$

the exact form of (52), (53) is recovered. (Recall that λ_j are defined by (28)–(32).)

Thus for the present $\tilde{G}(p)$ and A, the unknown function $f(p)$ can be determined from the dual integral equations by Tranter's method, and subsequently via (58) the function α is obtained. Next, application of (44), (39), (40) provides the functions under the integrals in (35)–(37), whose numerical evaluation renders the flow-field variables.

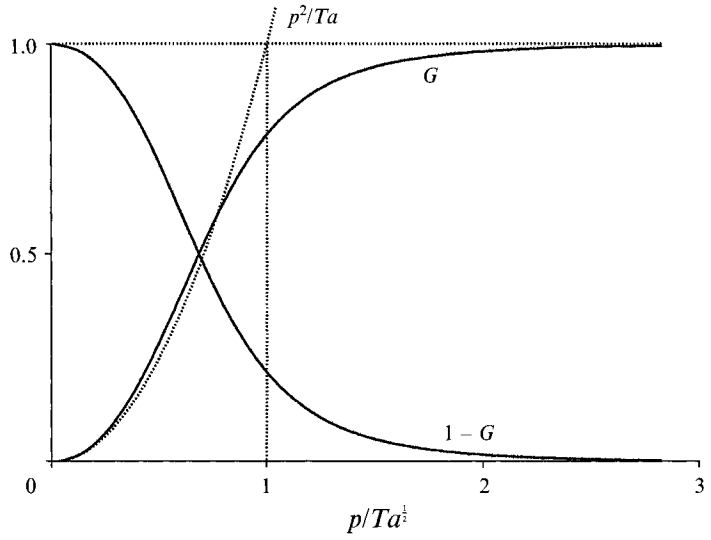

FIGURE 1. Graph of functions G, $1-G$ and p^2/Ta *vs.* $p/Ta^{\frac{1}{2}}$.

The essential task in the evaluation of $f(p)$ is the calculation of the improper integrals (57), which depend on $\tilde{G}(p)$. Since λ_j are functions of s only, where $s = 4Ta^2/p^4$, invoking (58)–(60), the following representation is evident:

$$\tilde{G}(p) = \frac{1}{p} G(s). \tag{61}$$

The behaviour of G is shown in figure 1; in general

$$G(s) > 0, \quad 0 < 1 - G(s) < s, \tag{62}$$

and in particular

$$G(s) = 2s^{-\frac{1}{2}} + \sqrt{2}s^{-\frac{3}{4}} + O(s^{-1}) \quad \text{for} \quad s \to \infty. \tag{63}$$

On account of (62) it can be concluded from (57) that the best rate of convergence for $L_{n,m}$ is attained by $k = \frac{1}{2}$, which motivates the choice of k in the subsequent analysis; we shall see later that this value of k also satisfies an important physical requirement.

3. Drag

Denoting again by T and by B the upstream and downstream flow regions, we write the formula for the drag, D:

$$D = \iint (P^T - P^B)\, \mathrm{d}S = 2\pi \int_0^1 r[P^T(r, z = 0^+) - P^B(r, z = 0^-)]\, \mathrm{d}r. \tag{64}$$

Only pressure (form) drag occurs on the disk, because clearly the shear terms on the surface $z = \text{const}$ cannot contribute to the force in the axial direction, and the vanishing thickness eliminates the shear contribution from the circumference, $r = 1$. In view of the antisymmetry of pressure, see (46), (47) and (58)–(60),

$$D = 4\pi \int_0^1 rP(r, z = 0^+)\, \mathrm{d}r = 4\pi \int_0^\infty f(p) \int_0^1 J_0(pr)\, r\, \mathrm{d}r\, \mathrm{d}p. \tag{65}$$

Application of the relationship

$$\int J_0(x)\,x\,\mathrm{d}x = xJ_1(x) \tag{66}$$

yields the compact result

$$D = 4\pi \int_0^\infty f(p)\frac{J_1(p)}{p}\,\mathrm{d}p. \tag{67}$$

On account of (54), with $k = \frac{1}{2}$, (67) takes the form

$$D = 4\pi \sum_{i=0}^{\infty} a_i \int_0^\infty \frac{J_{2i+\frac{1}{2}}(p)\,J_1(p)}{p^{\frac{1}{2}}}\,\mathrm{d}p. \tag{68}$$

For $i = 0$ the integral in (68) reduces to a standard one (Abramowitz & Stegun 1964, (11.4.35)):

$$\int_0^\infty \frac{J_{\frac{1}{2}}(p)\,J_1(p)}{p^{\frac{1}{2}}}\,\mathrm{d}p = \left(\frac{2}{\pi}\right)^{\frac{1}{2}} \int_0^\infty \frac{J_1(p)\sin(p)}{p}\,\mathrm{d}p = \left(\frac{2}{\pi}\right)^{\frac{1}{2}}. \tag{69}$$

In view of the formula (Watson 1952, p. 403)

$$\int_0^\infty \frac{J_\mu(t)\,J_\nu(t)}{t^\lambda}\,\mathrm{d}t = \frac{\Gamma(\lambda)\,\Gamma(\frac{1}{2}(\mu+\nu-\lambda+1))}{2^\lambda \Gamma(\frac{1}{2}(\mu-\nu+\lambda+1))\,\Gamma(\frac{1}{2}(\nu+\mu+\lambda+1))\,\Gamma(\frac{1}{2}(\nu-\mu+\lambda+1))}, \tag{70}$$

which is valid provided $\mu+\nu+1 > \lambda > 0$, one obtains

$$\int_0^\infty \frac{J_{2i+\frac{1}{2}}(p)\,J_1(p)}{p^{\frac{1}{2}}}\,\mathrm{d}p = 0 \quad \text{for} \quad i \geqslant 1. \tag{71}$$

Thus (68) reduces to

$$D = 4(2\pi)^{\frac{1}{2}} a_0. \tag{72}$$

For the evaluation of the drag a simple computer program, which uses standard Bessel function and integration routines, was devised. The infinite system (55), (56) was truncated to $N = 5$ equations; this gives three digits of accuracy in D, as concluded from numerical tests with N up to 20. Actually, this truncation is a critical issue of the solution, as discussed and validated later. The results of computations are presented in tables 1–3. Also shown in these tables are the corresponding results for drag on the sphere of Weisenborn (1985). For the sake of discussion it is convenient to consider separately the following ranges of Ta.

3.1. *Small Ta*

Enlightening and accurate approximations of the coefficient a_0 can be obtained for $Ta \to 0$, which turn out to be valid even for $Ta \approx 1$. The procedure here is an asymptotic evaluation of the exact solution, in contrast to the singular perturbation solution of the equations of motion that was used by Childress (1964) to obtain similar results.

The main task in the solution of (55), (56) with $k = \frac{1}{2}$ is the calculation of (57), i.e.

$$L_{n,m} = (4n+1)\int_0^\infty \frac{1}{p}(G(s(p))-1)\,J_{2m+\frac{1}{2}}(p)\,J_{2n+\frac{1}{2}}(p)\,\mathrm{d}p, \tag{73}$$

for $m, n = 0, 1, \ldots N$. It can be shown, see Appendix A, that

(*a*) for $Ta \to 0$,

$$L_{n,m} = O(Ta^{\frac{3}{2}}) \quad \text{for} \quad m+n \geqslant 1; \tag{74}$$

$$L_{0,0} = -\kappa\, Ta^{\frac{1}{2}} + O(Ta^{\frac{3}{2}}), \tag{75}$$

where
$$\kappa = 0.485; \tag{76}$$

(*b*) for an arbitrary value of Ta,

$$|L_{n,m}| \leqslant \frac{O(Ta^2)\,n}{(\max[n,m])^2} \quad \text{for} \quad m+n \gg 1. \tag{77}$$

The solution of (55), (56) is attempted in view of (74)–(77). Denoting by $\boldsymbol{L}$ the matrix of coefficients $(L_{n,m})$ and by $\boldsymbol{I}$ the identity matrix, the formal solution is

$$\begin{pmatrix} a_0 \\ a_1 \\ \vdots \\ a_n \\ \vdots \end{pmatrix} = (\boldsymbol{I}+\boldsymbol{L})^{-1} \begin{pmatrix} \frac{2\sqrt{2}}{\pi^{\frac{1}{2}}} \\ 0 \\ \vdots \\ 0 \\ \vdots \end{pmatrix} \tag{78}$$

The norm of $\boldsymbol{L}$, defined as $\max\{\sum_{m=0}^{\infty} L_{n,m}\}$ with respect to n, can be estimated: $\|\boldsymbol{L}\| = O(Ta^{\frac{1}{2}})$ as $Ta \to 0$. Hence it is justified for $Ta \ll 1$ to approximate the inverse matrix by

$$(\boldsymbol{I}+\boldsymbol{L})^{-1} = \boldsymbol{I}-\boldsymbol{L}+\boldsymbol{L}^2+O(\boldsymbol{L}^3); \tag{79}$$

consequently,

$$(\boldsymbol{I}+\boldsymbol{L})^{-1} = (1+0.485\,Ta^{\frac{1}{2}}+0.485^2 Ta)\boldsymbol{I}+O(Ta^{\frac{3}{2}}); \tag{80}$$

in particular, (78) and (80) yield

$$a_0 = \frac{2\sqrt{2}}{\pi^{\frac{1}{2}}}(1+0.485\,Ta^{\frac{1}{2}}+0.485^2 Ta+O(Ta^{\frac{3}{2}})). \tag{81}$$

Combining (81) and (72) one obtains that for $Ta \to 0$ the drag on the disk is

$$D = 16(1+0.485\,Ta^{\frac{1}{2}}+0.485^2 Ta+O(Ta^{\frac{3}{2}})). \tag{82}$$

The first interesting observation is that, for $Ta = 0$, (82) yields $D = 16$ (the dimensional form is obtained by multiplying with the scaling factor $\nu^*\rho^* a^* V^*$). This is exactly the classic, creeping-flow drag on a disk in a non-rotating flow, as given by (9).

Another interesting aspect of (82) follows from the comparison with Childress' (1964, equation (22)) result, obtained by a perturbation around the Stokes' solution, for a body of axial and fore-and-aft symmetry,

$$D_{body} = D^S_{body}\left(1+\frac{4}{7}\frac{D^S_{body}}{D^S_{sphere}}Ta^{\frac{1}{2}}\right)+O(Ta). \tag{83}$$

Here the subscript designates the geometry of the particle, and the superscript S denotes Stokes' drag on this body in non-rotating flow. Whence, according to (83), the drag on the disk on account of (9) and (8) is

$$D_{disk} = 16\left(1+\frac{32}{21\pi}Ta^{\frac{1}{2}}\right)+O(Ta). \tag{84}$$

Since $32/21\pi = 0.485$ the agreement between (84) and (82) is excellent.

The analysis of Weisenborn (1985) added one more term to (10):

$$D_{sphere} = 6\pi(1+\tfrac{4}{7}Ta^{\frac{1}{2}}+(\tfrac{4}{7})^2 Ta)+O(Ta^{\frac{3}{2}}). \tag{85}$$

Ta	(i) $\frac{D_{disk}}{D^S_{disk}}$	(ii) $\frac{D_{disk}}{D^S_{disk}}$	(iii) $\frac{D_{sphere}}{D^S_{sphere}}$	(iv) $\frac{D_{sphere}}{D^S_{sphere}}$
0.025	1.08	1.08	1.1	1.09 ± 0.01
0.1	1.17	1.17	1.21	1.22 ± 0.03
0.5	1.46	1.47	1.57	1.57 ± 0.05
1.0	1.72	1.74	1.9	—

TABLE 1. The drag for small Ta. (i) Approximate results for disk (82); (ii) 'exact' results for disk; (iii) Weisenborn's results for sphere; (iv) Maxworthy's experimental results for sphere

The perfect agreement between three independent outcomes (with respect to the first-order correction) attained by means of different techniques serves as a major *ad hoc* validation of the mathematical techniques employed in this study. Moreover, comparison among (82)–(85) leads to the conjecture that (83) can be extended by one more term, as follows:

$$D_{body} = D^S_{body}\left(1 + \frac{4}{7}\frac{D^S_{body}}{D^S_{sphere}} Ta^{\frac{1}{2}} + \left(\frac{4}{7}\frac{D^S_{body}}{D^S_{sphere}}\right)^2 Ta\right) + O(Ta^{\frac{3}{2}}). \tag{86}$$

It is also interesting to compare the analytical approximation of (82) with the 'exact' results, see table 1. The error naturally increases with Ta, but even for Ta as large as 1 it is still less than 2%. Thus, the asymptotic result (82) possesses high accuracy for $Ta \leqslant 1$.

The numerical solutions of Dennis *et al.* (1982) for $Ta \leqslant 0.5$, $Ro \leqslant 1$ and the experimental results of Maxworthy (1965) for $Ta \leqslant 0.75$ are in very good agreement with Weisenborn's calculations; this suggests that (82) and the generalized result (86) are also physically valid in this range of the parameters Ta and Ro.

3.2. *Moderate Ta*

The range of moderate values was defined here as $1 \leqslant Ta \leqslant 100$. Comparison in this intermediate range of Ta could be made only with the sphere drag results of Weisenborn (1985), see table 2. Both display the same dependency on Ta; the drag on the sphere (contributed by pressure and shear) is larger than on the disk, but the difference is reduced from approximately 30% to 15% as Ta increases from 1 to 100.

3.3. *Large Ta*

$Ta \geqslant 100$ can be considered 'large' because the flow field displays typical features of rapid rotation: a well-defined Taylor column and distinct Ekman layers, as discussed in the next section. The computations, however, could be carried out with satisfactory accuracy only up to about $Ta = 10000$, see table 3. Evidently, when Ta increases, the drag on the disk approaches the magnitude determined by Stewartson's formula (7), i.e. $D/Ta = 16/3 = 5.33$. (At $Ta = 10000$, the computed value is 5.31, slightly lower than the asymptotic one, probably due to round-off errors.) This 'exact' result is, versus classic approximations, of primary importance in the present investigation.

The drag on a sphere, calculated by Weisenborn (1985), is also shown in table 3. It is recalled that the drag on the disk is caused by the pressure difference, while on the sphere there is an additional contribution from the shear stresses. The results of table 3 support the anticipation that for large Ta the pressure distribution – hence the pressure (form) drag – on the disk and on the sphere are very close. It is seen that

Ta	(i) D_{disk}	(ii) D_{sphere}
1	27.9	35.8
2.5	39.1	50.9
5	56.0	70.4
7.5	72.0	93.0
10	87.6	112
25	177	217
50	320	379
75	459	533
100	597	686

TABLE 2. The drag for intermediate Ta: (i) for disk (present results); (ii) for sphere (from Weisenborn)

Ta	(i) $\frac{D_{disk}}{Ta}$	(ii) $\frac{D_{sphere}}{Ta}$	(iii) $\frac{16}{3}\left(1+\frac{2.7}{Ta^{\frac{1}{2}}}\right)$
100	5.97	6.86	6.77
250	5.66	6.26	6.24
500	5.52	5.98	5.98
750	5.47	5.86	5.86
1000	5.44	5.79	5.79
3000	5.36	—	—
6000	5.34	—	—
10000	5.31	5.47	5.48
100000	—	5.38	5.38

TABLE 3. The drag for large Ta: (i) for disk (present results); (ii) for sphere (from Weisenborn); (iii) for sphere, fitted formula

Weisenborn's results also approach asymptotically the prediction (7). However, these results suggest the fitting $D = \frac{16}{3}Ta(1+2.7Ta^{-\frac{1}{2}})$, see table 3, while the disk drag seems to behave like $D = \frac{16}{3}Ta(1+O(Ta^{-l}))$ with $l > \frac{1}{2}$. It was not possible to accurately determine l, but analysis of pressure in §4 suggests $l = \frac{3}{4}$ (see (97)).

4. Flow field

The description of the flow field is given in terms of the stream function in the meridional plane, see (48), angular velocity $\omega = v/r$, see (35), and pressure, see (45). Because of symmetry (asymmetry) of the flow-field variables with respect to the plane of the disk, only the upper half-space $z \geqslant 0$ is considered.

Figure 2 shows stream lines for increasing values of Ta. Qualitatively, the pattern does not change much when Ta varies from 0 to 10, as can be concluded from figure 2(*a*, *b*), except a tendency of the lines to concentrate toward the disk and the axis when Ta increases.

Further increase of Ta produces a distinct 'horizontal' Ekman layer over the disk, a 'vertical' shear layer, and a remarkable change of the flow close to the axis in the core (figures 2*c*, *d*). A qualitative novel feature appears when Ta attains approximately 37: the streamline $\psi = 0$ on the axis 'splits' above the disk to encompass a special region of trapped fluid, having the form of a bubble. With the growth of Ta the size of the 'bubble' quickly increases, (figure 2*e*, *f*).

Of special interest is the flow for large Ta; the following discussion is concerned with this range. The present calculations, carried out up to $Ta = 10000$, indicate the

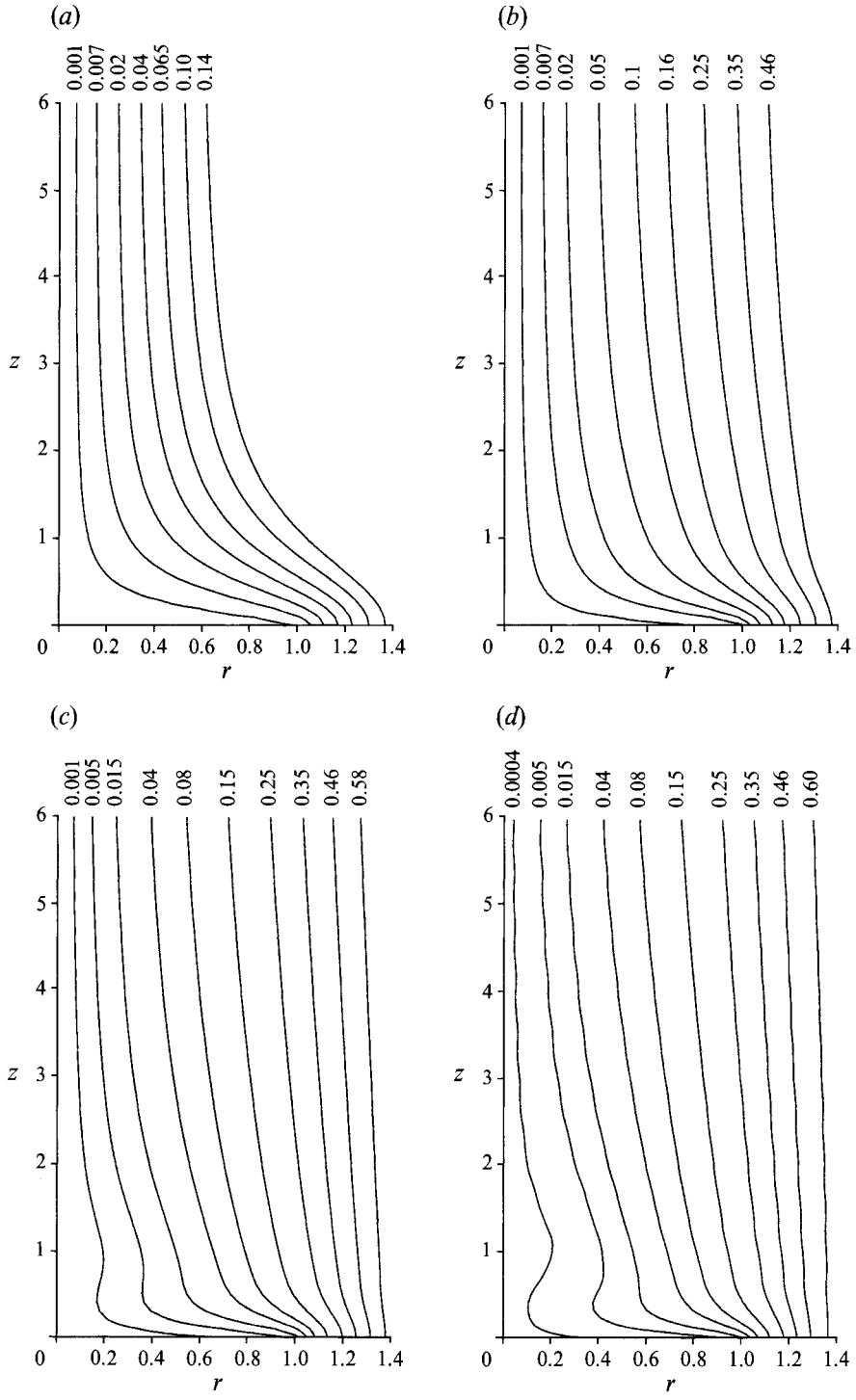

FIGURE 2(*a–d*). For caption see facing page.

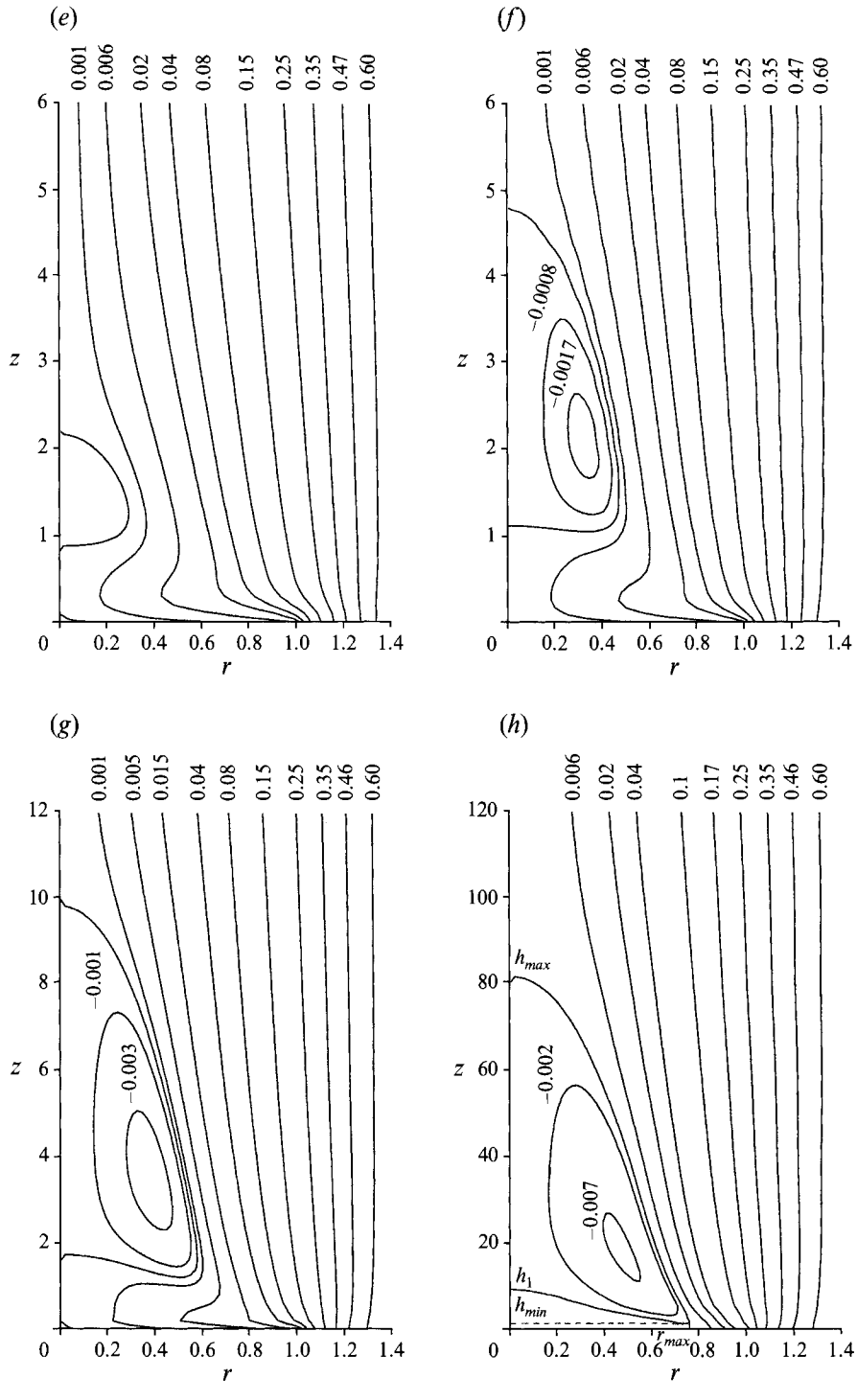

FIGURE 2. The contour lines of $-\psi$ for Ta values of (*a*) 0, (*b*) 10, (*c*) 25, (*d*) 35, (*e*) 50, (*f*) 100, (*g*) 200, (*h*) 1600.

following distinct results concerning the geometry of the recirculation 'bubble' and flow field when $Ta \to \infty$, figure 2(*g*, *h*). The highest point of the bubble is situated on the axis. At this point the axial velocity vanishes and the zero streamline bifurcates. The position of the point is

$$h_{max} \approx 5.1 \times 10^{-2} Ta. \tag{87}$$

The lowest point of the bubble on the axis, where the axial velocity vanishes once more, is characterized by $h_1 \approx 0.6 \times 10^{-2} Ta$. The lowest point of the bubble (here the axial velocity vanishes as well) is at $h_{min} > 1$; therefore, the bubble and the Ekman layer are well separated. The rightmost tip of the bubble approaches $r = 1$ (approximately $r_{max} \approx 1 - 1.5 \times Ta^{-\frac{1}{4}}$).

The fluid trapped in the bubble is in recirculating motion: it is not stagnant, but does not participate in the mass transfer around the particle. A convenient parameter to estimate the recirculation in the bubble is the maximal value of ψ inside, which increases with Ta to the asymptote of about 0.86×10^{-2}.

The fluid from upstream bends around the bubble and enters the zone below at $r = r_{max} = 1 - O(Ta^{-\frac{1}{4}})$. Consider now the region between the bubble and the body, bounded by the above-mentioned r_{max}. The fluid in this region is continuously supplied from the far field and subsequently drained by the Ekman layer. The axial velocity in this region is dominated by the Ekman layers and is $O(Ta^{-\frac{1}{2}})$.

Evidently, the 'column of liquid' observed by Taylor (1922) and the 'slug' of coloured fluid watched by Maxworthy (1970) should be identified as the projection of the envelope of the 'bubble' on the (r, z)-plane.

This gives rise to the following question: why did these investigators not report on the separating region between the body and the bubble? But a closer look will probably reverse the question to: what experiment is able to reveal this region? Actually, for an external observer, it is extremely difficult to see the fluid in the region $0 \leqslant r < r_{max}$, $h_{min} < z < h_1$, see figure 2(*h*), especially when the fluid in the bubble is dyed. Next, consider the region $0 \leqslant r \leqslant 1$, $0 \leqslant z < h_{min} = O(1)$. On a disk this fluid is amenable to observation, but its equivalent on the surface of an opaque sphere, as used by Taylor and Maxworthy (the disk is now, roughly, the equatorial plane) is, again, obscured. Consequently, even an extremely careful observer may reach the erroneous conclusion that the 'slug' is in direct contact with the Ekman layer on the surface of the sphere.

The present solution justifies the conjecture of Barnard & Pritchard (1975) that the length of the Taylor column is analytically determined by the farthest point on the axis where the axial velocity vanishes; they obtained, using Moore & Saffman's (1969) results, the distance $0.052Ta$, very close to the present $h_{max} = 0.051Ta$, and in good agreement with Maxworthy's value of $0.059Ta$.

The envelope of this Taylor column is stagnant with respect to the particle, but the velocity field inside requires attention. First, it is worth emphasizing that no drastic change of velocity or pressure across the boundary of the column was detected (in contradiction to Maxworthy's observation of a fast variation of w and P on the axis). Second, the 'inviscid' Taylor column solution (Stewartson 1952; Moore & Saffman 1969),

$$\omega = -\frac{2}{\pi} \frac{1}{(1-r^2)^{\frac{1}{2}}}, \quad w = 0, \quad u = 0, \quad r < 1, \tag{88}$$

which predicts that the fluid over the particle $r < 1$ moves with it as a whole body, is asymptotically valid in only a very small portion of the present column, $z \leqslant h_1$. For instance, on the axis, at $z \approx 0.03Ta$, we find $w \approx -0.2$ (i.e. of the order of magnitude of the free stream) and at $z = 0.04Ta$ we detect $\omega = 1.2$ (i.e. more than twice the prediction of (88)). Third, recall the recirculation with $\psi_{max} \approx 0.86 \times 10^{-2}$ inside the

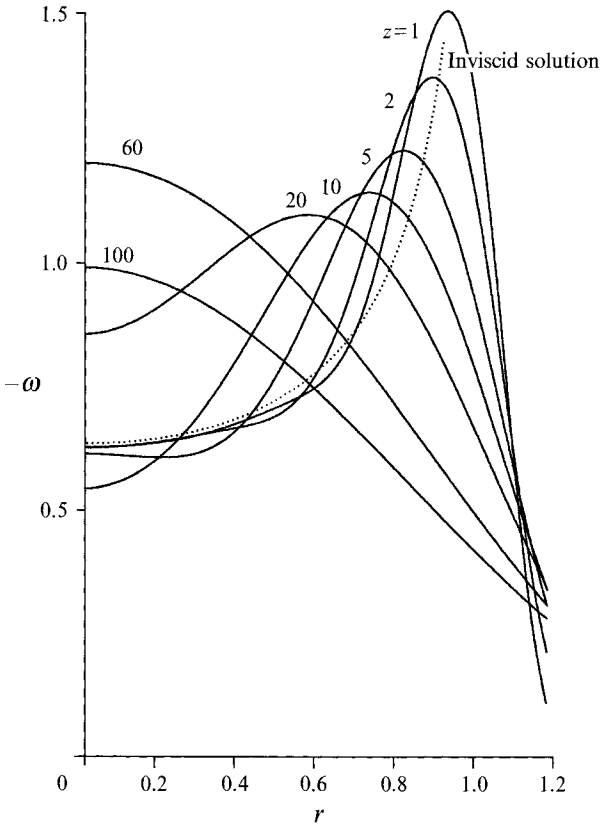

FIGURE 3. Angular velocities at various values of z; $Ta = 1600$.

bubble. The terms 'slug' or 'stagnant' for such a quite dynamic flow-field region may be misleading.

The values attained by the angular velocity, ω, are significantly higher in the bubble than predicted by the inviscid solution (88). Approaching the bubble on the axis from upstream we observe that ω increases up to approximately twice the value predicted by (88) at the middle of the bubble, then drops and remains practically constant and equal to (88) for $z < h_1$, see figure 3. This behaviour in the bubble region is in accordance with Maxworthy's observations; however, he reported a rather sharp variation of the variable around h_{max}.

Some interesting and novel features appear upon considering in some detail the pressure distribution on the disk, $z = 0$. By (47), (58)–(60), it reads

$$P(r, z = 0) = \int_0^\infty J_0(rp) f(p)\, \mathrm{d}p. \tag{89}$$

Considering the $p \to \infty$ limit and invoking the approximation

$$J_\nu(p) = \left(\frac{2}{\pi p}\right)^{\frac{1}{2}} \cos\left(p - \tfrac{1}{2}\nu\pi - \tfrac{1}{4}\pi\right) + O\left(\frac{1}{p}\right), \tag{90}$$

one can derive from (54) the asymptotic result

$$\begin{aligned} f(p) &\approx \left(\frac{2}{\pi p}\right)^{\frac{1}{2}} p^{1-k} \sum_{m=0}^{\infty} a_m \cos\left(p - \tfrac{1}{2}(2m+k)\,\pi - \tfrac{1}{4}\pi\right) \\ &= \left(\frac{2}{\pi}\right)^{\frac{1}{2}} p^{\frac{1}{2}-k} \cos\left(p - \tfrac{1}{2}k\pi - \tfrac{1}{4}\pi\right) \sum_{m=0}^{\infty} (-1)^m a_m. \end{aligned} \tag{91}$$

Introducing the notation,

$$\sigma = \left(\frac{2}{\pi}\right)^{\frac{1}{2}} \sum_{m=0}^{\infty} (-1)^m a_m, \tag{92}$$

and splitting the interval of integration in (89) at some $A_0 \gg 1$, yields

$$P(r, z=0) \approx \int_0^{A_0} J_0(rp) f(p)\, \mathrm{d}p + \sigma \int_{A_0}^{\infty} J_0(rp)\, p^{\frac{1}{2}-k} \cos\left(p - \tfrac{1}{2}k\pi - \tfrac{1}{4}\pi\right) \mathrm{d}p. \tag{93}$$

Analysis of (93) leads to important elucidation on two issues: (*a*) the 'proper' value of the parameter k, and (*b*) the contribution of the edge of the disk to the solution.

It is first recalled that the choice of the constant k in the expansion (54) is not determined by Tranter's method and remains rather arbitrary. The appropriate considerations in choosing k are the provision of:

(i) convergence of the integrals in (57);

(ii) existence of the solution for the infinite linear system (55), (56);

(iii) convergence of (54) for any p and, in particular, convergence of the series (92).

From the mathematical point of view, since the solution of the dual integral equation is apparently unique, k can virtually be chosen to make the best approximation of the solution (the norm here can be important). Whereas, as noticed by Tranter, his method of approximate solution lacks clear-cut recommendations on fixing k. The present approach employs the expected physical property of the solution to complete the mathematical method.

Thus (93) indicates a physical implication of k: it influences the type of singularity of P at the edge of the disk, $z = 0$, $r \to 1$. Indeed, for $k < 1$, (93) produces a singularity at the edge of the disk of the type $O((1-r)^{k-1})$. For $k > 1$ the integral represents a continuous function of r. It is important to notice that this behaviour of the result does not depend on the value of Ta, provided the series (92) converges.

On the other hand, the solution for the non-rotating case, $Ta = 0$, is known in closed form (Ray 1936); in particular

$$P(r, z=0) = \frac{4}{\pi} \int_0^{\infty} J_0(rp) \sin p\, \mathrm{d}p = \frac{4}{\pi} \frac{1}{(1-r^2)^{\frac{1}{2}}} \quad \text{for} \quad r < 1; \tag{94}$$

i.e. in the non-rotating case P has a singularity $O((1-r)^{-\frac{1}{2}})$. The singularity originates from the geometric configuration, i.e. the edge of the disk. At infinitesimally small distance from the edge, the flow-field structure (not the amplitude) must be determined by the edge, the effect of rotation (represented by Ta) being not of primary importance because the Coriolis terms there are much smaller than the viscous shear and pressure gradient. It is this consideration that leads to the conclusion that, from the physical point of view, the correct value of k is $\frac{1}{2}$, independent of Ta, for this particular problem.

Therefore (91) reads

$$f(p) = \sigma \sin p \quad \text{for} \quad p \gg 1; \tag{95}$$

and the formula (93) for pressure on the disk takes the form

$$\begin{aligned} P(r, z=0) &= \int_0^{A_0} J_0(rp)\, [f(p) - \sigma \sin p]\, \mathrm{d}p + \sigma \int_0^{\infty} J_0(rp) \sin p\, \mathrm{d}p \\ &= \int_0^{A_0} J_0(rp)\, [f(p) - \sigma \sin p]\, \mathrm{d}p + \frac{\sigma}{(1-r^2)^{\frac{1}{2}}}. \end{aligned} \tag{96}$$

Fast convergence of the first integral in (96) and the first term dominance in (54) in the vicinity of $p = 0$, when $k = \frac{1}{2}$, are used to estimate the order of magnitude of the pressure when $1 - r = O(1)$ (i.e. not near the edge); one finds that the second term

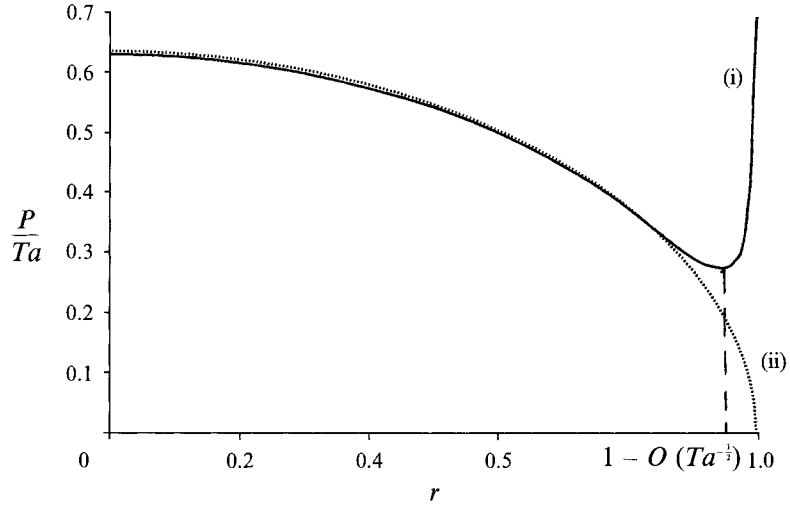

FIGURE 4. The pressure distribution on the surface of the disk: (i) present solution; (ii) inviscid solution.

becomes negligible for $Ta \gg 1$ and $P = O(a_0)$. On account of (72) and since the drag was shown to be of order Ta this means $P = O(Ta)$. Computations of pressure, plotted on figure 4, display excellent agreement of the present outcome with the inviscid solution, $P(r) = (2/\pi)\, Ta(1-r^2)^{\frac{1}{2}}$, for $(1-r) \geqslant O(Ta^{-\frac{1}{2}})$.

The second term in (96), however, is able to give a significant enhancement of pressure as $r \to 1$. Numerical evaluations give $\sigma = O(Ta^{\frac{1}{2}})$. So this effect becomes dominant if $(1-r) \leqslant O(Ta^{-\frac{1}{2}})$, as indeed confirmed by the computations, see figure 4.

It is interesting to note that with Ta increasing the magnitude of the singularity relative to the values in the core decreases like $Ta^{-\frac{1}{2}}$. The range governed by this singularity (wherein an inviscid pressure distribution is not valid) shrinks in the same proportion.

The large pressure on the disk at $r \to 1$ evidently enhances the drag over the inviscid result (7). The order of magnitude of this addition can be estimated as follows:

$$\Delta D = 4\pi \int_{1-O(Ta^{-0.5})}^{1} P(x, z = 0^+)\, \mathrm{d}r = 4\pi \int_{1-O(Ta^{-0.5})}^{1} \frac{\sigma}{(1-r^2)^{\frac{1}{2}}}\, \mathrm{d}r = O(Ta^{\frac{1}{4}}). \quad (97)$$

The relative excess $\Delta D/D$ appears to be of $O(Ta^{-\frac{3}{4}})$, less than the analogous one for a sphere which is of $O(Ta^{-\frac{1}{2}})$ according to Weisenborn's calculations. This estimate is also in agreement with the numerical drag calculation displayed in table 3.

Now the question of choosing k can be concluded. Physical considerations show that $k = \frac{1}{2}$. The rate of convergence of (57), as has been noticed, is best for $k = \frac{1}{2}$. However, for any other positive values of k these integrals also exist. But, following Kantorovich & Krylov (1964, Chap. 1) we verified that the 'generalized result' of Koch is applicable to (55), (56) with $k = \frac{1}{2}$, whatever Ta is, i.e. the solution a_m is unique and can be obtained as a limit of the solutions for truncated systems of N equations with N variables as $N \to \infty$. We were not able to show this *for any other* k by virtue of the same or some other theorem, and thereby to validate the entire procedure.

Finally, the rapid convergence of the coefficients a_m, and so that of the series (54), for $k = \frac{1}{2}$ is noted (see table 4), versus the not so favourable behaviour of a_m when solutions with different k were attempted.

Though some calculations here are very sensitive to the choice of k, the drag and

Ta	k	a_0	a_1	a_2	a_3	a_4	a_5	a_6	a_7	a_8	a_9	$\frac{D_{disk}}{Ta}$
1000	0.5	542	512	8.3	−5.4	3.5	−2	0.9	−0.3	0.05	0.01	5.44
1000	1.5	1559	−46	132	−189	188	−117	−9.5	152	−260	292	5.31
4000	0.5	2129	2079	15.5	−11	8	−6	4.5	−3	1.8	−0.9	5.34
4000	1.5	6231	79	27.7	−134	203	−211	148	−27	−117	234	5.27

TABLE 4. Coefficients of expansion (54) and the drag for $k = \frac{1}{2}$ and $\frac{3}{2}$

pressure in the core can be calculated, to the leading order, on the basis of k different from $\frac{1}{2}$. In this respect it should be mentioned that for the disk geometry the simplified equations of Greenspan (1968, §4.3) (time-dependent but with no viscosity) and Moore & Saffman (1969) (steady with Ekman layers neglected) were solved by a method equivalent to taking $k = \frac{3}{2}$ in Tranter's approach. In these cases only the leading term in the expansion (54) is non-zero and produces asymptotically, for $Ta \to \infty$, the correct solution for the simplified model without giving the correct type of singularity in the corner. Analogously, it appears that a finite number of terms in the expansion (54) with k different from $\frac{1}{2}$ cannot produce a solution uniformly valid in the whole space. Here as an *ad hoc* validation of this conjecture, a comparison between the coefficients a_m for $k = \frac{1}{2}$ and $k = \frac{3}{2}$ was performed and is displayed in table 4. One can judge the appropriate rate of convergence for a_m and reliability of numerical evaluations with respect to k.

The foregoing considerations, which lead to $k = \frac{1}{2}$ in (54) and in particular the approximation (95) with $\sigma = O(Ta^{\frac{1}{2}})$, make possible the evaluation of the 'corner' flow near the edge. Here the merging of the 'vertical' shear layer with the Ekman layer produces a delicate dynamical balance, which defies boundary-layer approximations.

On account of (37), (58)–(60) and (61) we write

$$w(r, z = 0) = -1 + \int_0^\infty J_0(rp) f(p) \frac{G(s)}{2p} \mathrm{d}p. \tag{98}$$

The objective is to estimate the order of magnitude of (98) with respect to Ta (recall, $w(z = 0, r) = 0$ for $r < 1$ and $w \to -1$ for $r \to \infty$). To this end the interval of integration was split in several subintervals where different asymptotics for the involved functions are available. The details are given in Appendix B. The conclusion is that the maximal attainable $w(r, z = 0)$ is $O(Ta^{\frac{1}{4}})$ at the distance $\delta = r - 1 = O(Ta^{-\frac{1}{2}})$ from the disk edge (see figure 5).

Similar but more complicated evaluations show that for $r = 1$, $|z| = O(Ta^{-\frac{1}{2}})$, w also attains values of order $Ta^{\frac{1}{4}}$. Subsequently, on account of (14) it can be derived that in the corner $r - 1 \approx |z| = O(Ta^{-\frac{1}{2}})$, u is also $O(Ta^{\frac{1}{4}})$. The same result for v from (12) leads to the conclusion that all velocity components are of the same order of magnitude in the 'corner' of size $O(Ta^{-\frac{1}{2}})$ around the edge. Numerical results, as shown on figure 6, confirm these estimates.

It is of some interest to compare the present evaluations of the 'corner' flow with those of Moore & Saffman (1969). In our notation their results for the axial velocity in the vertical shear layer ($\delta \ll 1$) read

$$w = -1 - \frac{1}{\pi^{\frac{3}{2}}} \left(\frac{2Ta}{z} \right)^{\frac{1}{6}} \int_0^\infty \mathrm{e}^{-p^3} \frac{\cos p\zeta + \sin p\zeta}{p^{\frac{1}{2}}} \mathrm{d}p, \tag{99}$$

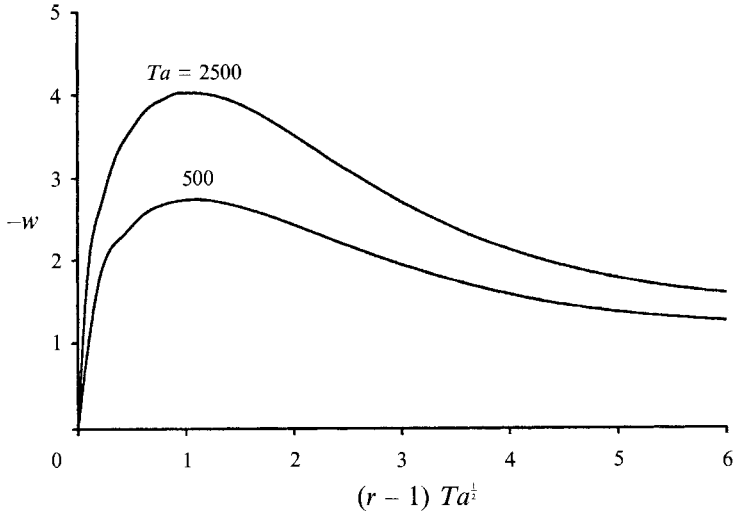

FIGURE 5. The axial velocities on the plane of the disk for two values of Ta.

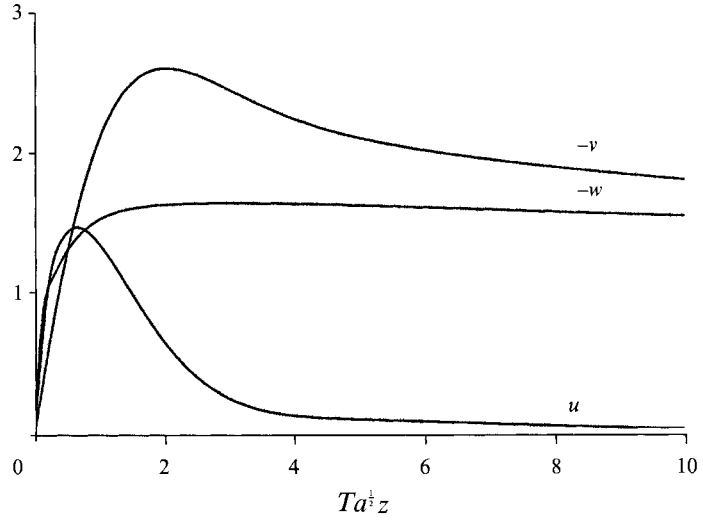

FIGURE 6. The radial, azimuthal and axial velocities u, v, w, *vs.* z at $r = 1$, $Ta = 5000$.

where $\zeta = \delta(2Ta/z)^{\frac{1}{3}}$. Although (99) was developed for $z \gg Ta^{-\frac{1}{2}}$, it turns out that it agrees in order of magnitude with the present result when $z = O(Ta^{-\frac{1}{2}})$. Comparison with the present solution beyond the Ekman layer displays fair agreement.

For $\delta < Ta^{-\frac{1}{2}}$ and $z \gg Ta^{-\frac{1}{2}}$ and so $\zeta \ll 1$ the integral in (99) is approximately a constant of the order of unity. Therefore, $w = O(Ta^{\frac{1}{3}})$ when $z = O(1)$ and grows till $w = O(Ta^{\frac{1}{4}})$ for $z = O(Ta^{-\frac{1}{2}})$. But on decreasing z an infinite growth shows up in (99), while in the present analysis w will remain bounded by $O(Ta^{\frac{1}{4}})$, actually tending to 0 as $z \to 0$ (the maximal value for $r = 1$ is attained when $z = O(Ta^{-\frac{1}{2}})$, see figure 6). A comparison for the azimuthal velocity leads to a similar conclusion.

5. Concluding remarks

The present 'exact' solution of the full linear equations facilitates the analysis of the flow field past a rising disk in the rotating fluid for the whole range of Taylor numbers. The rigour of the mathematical approach (Tranter's method of solving dual integral equations) is not sufficiently assessed at present, but the proof of the correctness of all the steps, comparison with the limiting cases and other *ad hoc* tests give strong support to the results.

For small values of Ta a small departure from the non-rotating case was noted, without change of the principal conventional features. The correction to the Stokes drag formula for a disk is of the same type as for a sphere (Childress 1964); actually, a simple and accurate drag correlation, (86), could be conjectured for a particle of quite general geometry (subject to axi- and fore-and-aft symmetry). There is both analytical and experimental evidence that the sensitivity of the drag on a sphere to Ro is small, thus the linear theory results are applicable for $Ro \leqslant 1$.

As the Taylor number Ta increases, the flow pattern begins to be modified: the shear effects tend to concentrate in Ekman and vertical shear layers, and a domain of recirculating fluid appears above (and below) the disk (approximately for $Ta = 37$). With further increase of Ta this domain quickly lengthens and widens, gaining the shape of a prolongated 'bubble', with a clearly defined envelope. It is quite evident that the trapped fluid in the bubble, plus the fluid flowing between it and the disk, can be identified as the experimentally observed 'Taylor column', or 'slug'. The length of this domain, $\approx 0.051\,Ta$, appears in good agreement with Maxworthy's (1970) measured size of the 'slug' and with the corresponding value calculated by Barnard & Pritchard (1975) from Moore & Saffman's (1969) solution.

On the other hand, the present results are in contrast to some of Maxworthy's interpretations of observations on the type of motion in this region. He theorized that the slug represented practically stagnant, very slowly moving fluid, supplying the Ekman-layer suction. It is seen here that the fluid sucked by the Ekman layer does not pass through the region of trapped fluid, rather goes around it, and the Ekman layer is separated from the bubble. The fluid in the bubble is purely recirculating and the corresponding velocities inside do not decay when $Ta \to \infty$. The recirculation feature of the flow finds some theoretical support in the *inviscid* models of Greenspan (1968, §4.3) and Miles (1972) and experimental confirmation in Orloff & Bossel (1971).

Recent investigations by Tanzosh & Stone (1994) and by H. A. Stone, J. Bloxham and J. W. M. Bush provide a sharper corroboration of these important flow field properties, as follows. First, the numerical solution based upon a boundary-integral-type formulation of the governing linear equations for a sphere displays qualitative and quantitative agreement with the present results (the bifurcation occurs at $Ta \approx 50$, *vs.* the present $Ta \approx 37$ for the disk). Second, in experiments with a silicone oil drop in water ($Ta \approx 10^4$, $Ro \approx 0.4$), visualization by kalliriscope indicated a recirculation in the forward 'wake' (the rear wake was affected by the proximity of the boundary).

It is interesting to compare the velocities calculated from the Moore & Saffman (1969) solution with the present ones. There is good agreement in the vertical shear layer, the upper part of the bubble and the flow above it. Obviously, the results are not comparable in the region of order $Ta^{-\frac{1}{3}}$ around the disk. Moreover, they also differ significantly in the zone influenced by the Ekman suction over the disk, and also in the lower part of the bubble. Therefore, the omission of Ekman suction defies a clearcut analytical definition of the Taylor column boundaries.

To evaluate the corner flow it was necessary to determine the correct value of the constant k which is employed in Tranter's method. The principle that the type of the

pressure singularity at the corner is determined by the geometry of the configuration and is independent of Ta was suggested. On this basis it was estimated that the maximal values of the velocities are attained around the edge of the disk and their order or magnitude is $Ta^{\frac{1}{4}}$. This is consistent with Maxworthy's observations that in the range of parameters in his experiments ($Ta = O(1000)$) the enhancement of the axial velocity over the free-stream value is 25–50%.

The present calculations of the drag are consistent with the previous ones, i.e. for large Ta and zero Ro the drag on a sphere in an infinite domain is $\frac{16}{3}Ta$, as calculated by Stewartson (1952), with a relative error of probably $O(Ta^{-\frac{1}{2}})$ at most. On the other hand, Maxworthy (1970) concluded, by smoothing and extrapolating experimental data, that for large Ta and small Ro the drag is 53% larger than the linear result.

The conclusion is that for large Ta the linear theory, augmented by the present incorporation of the Ekman layers, when compared with experiments (at small Ro), displays agreement in many flow-field features, but a significant discrepancy in the drag.

Since the analysis of Hocking *et al.* (1979) on the influence of the endcaps of the container and the present investigation on the effect of the Ekman layers† fail to explain the 53% discrepancy between Stewartson's result and Maxworthy's correlation, the only apparent deficiency in the theory, to which the disagreement can be attributed, remains the omission of the non-linear terms.

This explanation is, however, not easy to accept. The basic assumption is that the linear theory, with $Ro = 0$, provides the leading term in some expansion in powers of Ro; therefore, it should be a fair approximation for small but finite Ro, provided the neglected terms are smaller than the retained ones. Moreover, for a fixed Ta, the accuracy of the approximation is expected to improve smoothly with the decrease of Ro. In the present linear solution no non-uniformities associated with the infinity of the domain (cf. Stokes' flow) have been detected. The local non-uniformities appearing in the vertical shear layers seem unable to affect substantially the solution in the range of Maxworthy's experiments. A careful inspection (Hocking *et al.* 1979, §6) indicates that, for $Ro < 10^{-2}$ and $Ta \approx 10^2$–10^3, the nonlinear neglected terms are still only several percent of the leading ones. This stringent examination also reveals two disturbing trends in Maxworthy's experimental results: (*a*) the scattering with respect to Ro is large when $Ro = O(10^{-2})$; (*b*) the discrepancy with theory increases when Ro is reduced.

These conflicting circumstances cast some doubt on the interpretation of the available experimental data and, in particular, on their extrapolation and smoothing that led to the conclusion that the real drag is 53% higher than predicted by the linear theory. An independent experimental verification is necessary. If the previous experimental findings are confirmed we shall apparently face another fluid dynamics 'paradox', see Goldshtik (1990), in the sense that the slightest, unavoidable, presence of momentum convection gives rise to a significant deviation from the linear flow field around the slowly rising sphere.

We thank Professor A. Sidi for his help in the interpretation and evaluation of some improper integrals encountered in the present investigation. The research was partially supported by the Fund for the Promotion of Research at the Technion, and D.V. was

† The assumption is that these results can be superposed. The more physical model of an axially bounded domain with Ekman layers accounted for is presently under investigation.

partially supported by the Bat Sheva de Rothschild Foundation for the Advancement of Science in Israel & Co.

Appendix A. Justification of the estimates (74), (75) and (77)

Consider first (75) and assume $Ta \ll 1$. In view of the identity

$$J_{\frac{1}{2}}(p) = (2/\pi p)^{\frac{1}{2}} \sin p \tag{A 1}$$

$L_{0,0}$ reads

$$L_{0,0} = \int_0^\infty \frac{1}{p}(G(s(p))-1)\, J_{\frac{1}{2}}(p)\, J_{\frac{1}{2}}(p)\, \mathrm{d}p = \frac{2}{\pi}\int_0^\infty (G(s(p))-1)\frac{\sin^2 p}{p^2}\mathrm{d}p$$

$$= \frac{2}{\pi}\int_0^\infty (G(s(p))-1)\,\mathrm{d}p - \frac{2}{\pi}\int_0^\infty (G(s(p))-1)\frac{p^2-\sin^2 p}{p^2}\mathrm{d}p. \tag{A 2}$$

The change of the variable $p = (2Ta)^{\frac{1}{2}} s^{-\frac{1}{4}}$ in the first integral of (A 2) results in

$$\frac{2}{\pi}\int_0^\infty (G(s(p))-1)\,\mathrm{d}p = \frac{1}{\sqrt{2\pi}}\, Ta \int_0^\infty s^{-\frac{5}{4}}(G(s)-1)\,\mathrm{d}s = -\kappa T a^{\frac{1}{2}}. \tag{A 3}$$

Convergence of the last integral is readily verified and numerical evaluation provides $\kappa = 0.485$.

The second integral of (A 2) can be easily estimated after splitting the interval in three by $Ta^{\frac{1}{2}}$ and 1. In view of the bounds (see (62))

$$1 - G(s) < s = 4Ta^2/p^4, \tag{A 4}$$

$$0 < G(s) < 1, \quad 0 \leqslant p^2 - \sin^2 p \leqslant p^4 \tag{A 5}$$

the following estimates are readily produced:

$$0 \leqslant \int_0^{Ta^{\frac{1}{2}}} (1-G(s))\frac{p^2-\sin^2 p}{p^2}\mathrm{d}p \leqslant \int_0^{Ta^{\frac{1}{2}}} p^2\,\mathrm{d}p = \tfrac{1}{3}Ta^{\frac{3}{2}}, \tag{A 6}$$

$$0 \leqslant \int_{Ta^{\frac{1}{2}}}^1 (1-G(s))\frac{p^2-\sin^2 p}{p^2}\mathrm{d}p \leqslant 4\int_{Ta^{\frac{1}{2}}}^1 \frac{Ta^2}{p^4}p^2\,\mathrm{d}p = 4(Ta^{\frac{3}{2}} - Ta^2), \tag{A 7}$$

$$0 \leqslant \int_1^\infty (1-G(s))\frac{p^2-\sin^2 p}{p^2}\mathrm{d}p \leqslant \int_1^\infty 4\frac{Ta^2}{p^4}\mathrm{d}p = \tfrac{4}{3}Ta^2. \tag{A 8}$$

Thus, the result (75) is recovered:

$$L_{0,0} = -0.485\, Ta^{\frac{1}{2}} + O(Ta^{\frac{3}{2}}). \tag{A 9}$$

The proof of (74) is similar.

To obtain (77) the interval of integration is split in two by $p = (\max(n,m))^{\frac{1}{2}} \gg 1$. For definiteness, suppose $n \geqslant m$. On the second subinterval in view of (A 4) and the inequality $J_\nu(p) \leqslant 1$ one readily has

$$\left|\int_{n^{\frac{1}{2}}}^\infty \frac{(1-G(s))}{p} J_{2m+\frac{1}{2}} J_{2n+\frac{1}{2}}\mathrm{d}p\right| \leqslant \int_{n^{\frac{1}{2}}}^\infty 4\frac{Ta^2}{p^5}\mathrm{d}p = \frac{Ta^2}{n^2}. \tag{A 10}$$

On the first subinterval, since the power series expansion for $J_{2n+\frac{1}{2}}(p)$ is of Leibniz type, the following estimate is employed:

$$J_\nu(p) \leqslant \frac{p^\nu}{2^\nu \Gamma(\nu+1)}. \tag{A 11}$$

Other factors are bounded as on the second subinterval, hence

$$\left|\int_0^{n^{\frac{1}{2}}} \frac{(1-G(s))}{p} J_{2m+\frac{1}{2}} J_{2n+\frac{1}{2}} \mathrm{d}p\right| \leqslant \int_0^{n^{\frac{1}{2}}} 4\frac{Ta^2}{p^5} \frac{p^{2n+\frac{1}{2}}}{2^{2n+\frac{1}{2}}\Gamma(2n+\frac{3}{2})} \mathrm{d}p$$

$$= Ta^2 \frac{n^{n-\frac{7}{4}}}{(2n-\frac{7}{2})\,2^{2n-\frac{3}{2}}\Gamma(2n+\frac{3}{2})} = Ta^2 o\left(\frac{1}{n^2}\right). \tag{A 12}$$

In the last step Stirling's formula was used. Combining (A 10) and (A 12), and interchanging m, n if $m > n$, yields (77).

Appendix B

The velocity w for $z = 0$, expressed by (98), is amenable to an order-of-magnitude analysis with respect to Ta, for $Ta \to \infty$. Let I_0, I_1 and I_2 be the contributions of the intervals $[0, A_1]$, $[A_1, A_2\, Ta^{\frac{1}{2}}]$ and $[A_2\, Ta^{\frac{1}{2}}, \infty]$.

We start by evaluating the contribution of the interval $[A_1, A_2\, Ta^{\frac{1}{2}}]$ ($A_1 \gg 1$, $A_2 \ll 1$), wherein (63) and (90) both are asymptotically valid. On account of (95), let

$$I_1 = \int_{A_1}^{A_2 Ta^{\frac{1}{2}}} J_0(rp) f(p) \frac{G(s)}{2p} \mathrm{d}p \approx \int_{A_1}^{A_2 Ta^{\frac{1}{2}}} \left(\frac{2}{\pi rp}\right)^{\frac{1}{2}} \cos(rp - \tfrac{1}{4}\pi)\, \sigma \frac{p}{2Ta} \sin p \,\mathrm{d}p$$

$$= \frac{\sigma}{2Ta(2\pi r)^{\frac{1}{2}}}\left[\int_{A_1}^{A_2 Ta^{\frac{1}{2}}} p^{\frac{1}{2}} \sin(p(1+r) - \tfrac{1}{4}\pi)\,\mathrm{d}p + \int_{A_1}^{A_2 Ta^{\frac{1}{2}}} p^{\frac{1}{2}} \sin(p(1-r) + \tfrac{1}{4}\pi)\,\mathrm{d}p\right]. \tag{B 1}$$

The first integral can be shown to be $o(1)$ and thus is negligible in the present consideration. Keeping the second and denoting $\delta = r - 1$, we get

$$I_1 \approx \frac{\sigma}{4Ta(\pi r)^{\frac{1}{2}}} \int_{A_1}^{A_2 Ta^{\frac{1}{2}}} p^{\frac{1}{2}} [\cos p\delta - \sin p\delta]\,\mathrm{d}p$$

$$= \frac{\sigma}{4Ta(\pi r)^{\frac{1}{2}}} \delta^{-\frac{3}{2}} \int_{A_1\delta}^{A_2\delta Ta^{\frac{1}{2}}} q^{\frac{1}{2}} [\cos q - \sin q]\,\mathrm{d}q. \tag{B 2}$$

For $\delta = O(1)$, since $\sigma = O(Ta^{\frac{1}{2}})$, after integration by parts $I_1 = o(1)$. For $\delta < Ta^{-\frac{1}{2}}$ approximately

$$I_1 = \frac{\sigma}{4Ta(\pi r)^{\frac{1}{2}}} \delta^{-\frac{3}{2}} \int_{A_1\delta}^{A_2\delta Ta^{\frac{1}{2}}} q^{\frac{1}{2}} [\cos q - \sin q]\,\mathrm{d}q$$

$$= \frac{\sigma}{4Ta(\pi r)^{\frac{1}{2}}} \tfrac{2}{3} A_2^{\frac{3}{2}} Ta^{\frac{3}{4}} = O(Ta^{\frac{1}{4}}). \tag{B 3}$$

It is readily seen that for $Ta^{-\frac{1}{2}} \ll \delta \ll 1$, $O(1) \ll I_1 \ll Ta^{-\frac{1}{4}}$, i.e. the maximal values of I_1 are of order $Ta^{-\frac{1}{4}}$ and attained at distance of order $Ta^{-\frac{1}{2}}$ from the rim.

Although these estimates are asymptotically correct provided $A_2 \to 0$, their validity is expected to hold for order-of-magnitude evaluation also when $A_2 = 1$, see figure 1.

On the other hand, in a similar manner letting $A_2 \gg 1$, when $s \ll 1$ and $G(s) \approx 1$ by (62), we get

$$I_2 = \int_{A_2 Ta^{\frac{1}{2}}}^{\infty} J_0(rp) f(p) \frac{G(s)}{2p} \mathrm{d}p$$

$$\approx \frac{\sigma}{4(\pi r)^{\frac{1}{2}}} \int_{A_2 \delta Ta^{\frac{1}{2}}}^{\infty} \frac{\cos q - \sin q}{q^{\frac{3}{2}}} \mathrm{d}q, \tag{B 4}$$

which shows the same order of magnitude with respect to δ as I_1. Repeating the analysis similar to the one for I_1 and letting $A_2 = 1$ reproduces the same outcome.

It can be easily shown that I_0 is of order 1 because $A_1 = O(1)$ and the leading term $a_0 = O(Ta)$ in (54) is dominant. Thus, the maximal attainable $w(r, z = 0)$ is $O(Ta^{\frac{1}{4}})$ at the distance $\delta = O(Ta^{-\frac{1}{2}})$ from the disk edge ($\delta > 0$). Apparently for $\delta < 0$ the considered balance results in $w = 0$, the contributions of order $O(Ta^{\frac{1}{4}})$ from I_1 and I_2 cancel out.

REFERENCES

ABRAMOWITZ, M. & STEGUN, I. A. 1964 *Handbook of Mathematical Functions*. Dover.

BARNARD, B. J. S. & PRITCHARD, W. G. 1975 The motion generated by a body moving through a stratified fluid at large Richardson numbers. *J. Fluid Mech.* **71**, 43–64.

CHILDRESS, S. 1964 The slow motion of a sphere in a rotating, viscous fluid. *J. Fluid Mech.* **20**, 305–314.

DENNIS, C. R., INGHAM, D. B. & SINGH, S. N. 1982 The slow translation of a sphere in a rotating viscous fluid. *J. Fluid Mech.* **117**, 251–267.

GOLDSHTIK, M. A. 1990 Viscous-flow paradoxes. *Ann. Rev. Fluid Mech.* **22**, 441–472.

GREENSPAN, H. P. 1968 *The Theory of Rotating Fluids*. Cambridge University Press.

HOCKING, L. M., MOORE, D. W. & WALTON, I. C. 1979 The drag on a sphere moving axially in a long rotating container. *J. Fluid Mech.* **90**, 781–793.

KANTOROVICH, L. V. & KRYLOV, V. I. 1964 *Approximate Methods of Higher Analysis*. Interscience.

MAXWORTHY, T. 1965 An experimental determination of the slow motion of a sphere in a rotating, viscous fluid. *J. Fluid Mech.* **23**, 373–384.

MAXWORTHY, T. 1970 The flow created by a sphere moving along the axis of a rotating, slightly-viscous fluid. *J. Fluid Mech.* **40**, 453–479.

MILES, J. W. 1972 Axisymmetric rotating flow past a circular disk. *J. Fluid Mech.* **53**, 689–700.

MOORE, D. W. & SAFFMAN, P. G. 1969 The structure of free vertical shear layers in a rotating fluid and the motion produced by a slowly rising body. *Phil. Trans. R. Soc. Lond.* A **264**, 597–634.

MORRISON, J. W. & MORGAN, G. W. 1956 The slow motion of a disk along the axis of viscous, rotating liquid. *Rep.* 56207/8. Div. of Appl. Maths, Brown University.

ORLOFF, K. & BOSSEL, H. 1971 Laser-Doppler velocity measurements of swirling flows with upstream influence. *Bull. Am. Phys. Soc.* **16**(2), 1331 (abstract only).

RAY, M. 1936 Application of Bessel functions in the solution of problems of motion of a circular disk in viscous liquid. *Phil. Mag.* (7) **21**, 546–564.

STEWARTSON, K. 1952 On the slow motion of an ellipsoid in a rotating fluid. *Q. J. Mech. Appl. Maths* **6**, 141–162.

TANZOSH, J. & STONE, H. A. 1994 Motion of a rigid particle in a rotating viscous flow: An integral equation approach. Submitted.

TAYLOR, G. I. 1922 The motion of a sphere in a rotating liquid. *Proc. R. Soc. Lond.* A **102**, 180–189.

TRANTER, C. J. 1951 *Integral Transforms in Mathematical Physics*. Methuen.

UNGARISH, M. 1993 *Hydrodynamics of Suspensions: Fundamentals of Centrifugal and Gravity Separation*. Springer.

WATSON, G. N. 1952 *A Treatise on the Theory of Bessel Functions*. Cambridge University Press.

WEISENBORN, A. J. 1985 Drag on a sphere moving slowly in a rotating viscous fluid. *J. Fluid Mech.* **153**, 215–227.